

Supporting Information

Dendrite-Free and Stable anode for High-performance Li–O₂ Batteries by prestoring Li into Reduced Graphene Oxide coating Three-Dimensional Nickel Foam

Huimin Zhao,^{a‡} Yiru Ma,^{a‡} Haocheng Qi,^a Zhenyu Xiao,^a Haifeng Lin,^a Jie Liu,^b
Ziyang Guo,^{a*} Lei Wang^{a*} and Shouhua Feng^c

a Key Laboratory of Eco-chemical Engineering, Taishan scholar advantage and characteristic discipline team of Eco chemical process and technology, College of Chemistry and Molecular Engineering, Qingdao University of Science and Technology, Qingdao 266042, P. R. China.

b Key Laboratory of Eco-chemical Engineering, Taishan scholar advantage and characteristic discipline team of Eco chemical process and technology, College of Chemical Engineering, Qingdao University of Science and Technology, Qingdao 266042, P. R. China.

c State Key Laboratory of Inorganic Synthesis and Preparative Chemistry of Jilin University

** Corresponding author. Tel & Fax: 0086-0532-84023409*

E-mail address: inorchemwl@126.com (Wang L); zyguo@qust.edu.cn (Guo Z)

‡ Huimin Zhao and Yiru Ma contributed equally to this work.

Material Preparation

Materials

Tetraethylene glycol dimethyl ether (TEGDME, 99.9 %), LiTFSI (Sigma-Aldrich, 99.95 %), pyrrole and 50 wt% phytic acid solution (w/w) in H₂O were purchased from Sigma-Aldrich. 1.0 M bis (trifluoromethane) sulfonamide lithium salt (LiTFSI) in 1:1 v/v dimethoxyethane (DME) and 1, 3-dioxolane (DOL) with 2.0 wt% lithium nitrate (LiNO₃) additive, and 1.0 M LiTFSI in 1:1 v/v DME and DOL with 2.0 wt% LiNO₃ was obtained from Duoduo Reagent. Trimethylolpropaneethoxylatetriacrylate (average Mn of ~428), 2-hydroxy-2-methyl-1-phenyl-1-propanone (C₆H₅COC(CH₃)₂OH, 97%), and poly(vinylidene fluoride-co-hexafluoropropylene) (average Mn of ~130000) were purchased from Sigma-Aldrich. Ketjenblack (EC600JD) produced by Shanghai Tengmin Industry Co., Ltd. N-methyl-2-pyrrolidinone (C₅H₉NO, 99 %) was purchased from Aladdin Reagent. Na₂CO₃ (99.8 %) and RuCl₃•xH₂O were purchased from Aladdin Reagent. Carbon paper was TGP-H-060 carbon paper. Other chemicals were from Sinopharm Chemical Reagent Corp. All chemicals were used as received without further purification.

Preparation of Li/rGO-Ni electrode

Firstly, Ni foam was cut into square pieces with area of 1 cm² and washed successively with 1 M hydrochloric acid, acetone, and ethanol for 15 minutes, respectively. Then, these square Ni films were finally dried overnight in vacuum drying oven. After that, cleaned Ni foam was repeatedly soaked with 5 wt% GO solution for several times and then dried at 80 °C for 12 h to obtained GO modified Ni foam (denoted as GO-Ni). Before the thermal-infusion test, metallic Li was heated to ≈300 °C by a heating plate and then melted in the battery case. Finally, the molten Li was rapidly infused into the GO-Ni framework to form Li based reduced (r)GO-Ni (denoted as Li/rGO-Ni) electrode. GO has been reduced into rGO by the

high-temperature ($>150\text{ }^{\circ}\text{C}$, produced by molten Li). We mainly adjust the time of thermal-infusion process to control the amount of Li in rGO-Ni foam. The Li/rGO-Ni electrode with high Li amount (H-Li/rGO-Ni, $m_{\text{Li}} \approx 26\text{ mg cm}^{-2}$), the Li/rGO-Ni electrode with low Li amount L-Li/rGO-Ni ($m_{\text{Li}} \approx 7\text{ mg cm}^{-2}$), and Li/rGO-Ni anodes ($m_{\text{Li}} \approx 20\text{ mg cm}^{-2}$) were prepared. At the same time, the Li based Ni (Li/Ni) electrode has also been prepared for comparison, .

Assembly of batteries and electrochemical measurements

Firstly, symmetric batteries were assembled by sealing Li-based (Li/rGO-Ni, Li/Ni or Li) electrode, electrolyte (1.0 M bis(trifluoromethane) sulfonamide lithium salt (LiTFSI) in 1:1 v/v dimethoxyethane (DME) and 1, 3-dioxolane (DOL) with 2.0 wt % lithium nitrate (LiNO_3) additive) and Li/rGO-Ni (Li/rGO-Ni, Li/Ni or Li) electrode were sealed into CR2016-type coin configuration. For assembly of Li-O₂ full batteries, Ketjenblack (KB)/ruthenium (Ru) composite cathode|separators filled with electrolyte (1 M Bis(trifluoromethane) sulfonamide lithium salt (LiTFSI)/tetraglyme (TEGDME))|Li/rGO-Ni or pure Li anode were orderly sealed into into the Swagelok-type configuration (there is a hole of $\sim 0.8\text{ cm}^{-2}$ on the top side). Moreover, the fabrication of the flexible Li-O₂ batteries was summarized as follow: Li/rGO-Ni fiber was firstly prepared and used as inner anode. After that, the precursor solution of the gel polymer electrolyte (GPE) was coated on the surface of Li/rGO-Ni fiber and subsequently treated by UV irradiation for $\sim 60\text{ s}$. Then, the KB/Ru carbon rope cathode was enwound on the surface of GPE coated Li/rGO-Ni fiber anode. Finally, the above flexible Li-O₂ battery was sealed into a punched heat shrinkable tube. All

the above batteries were assembled in the pure Ar-filled glove box with O₂ and H₂O contents < 0.1 ppm. In addition, all the cells were cycled in the eight-channel LAND battery test system (Wuhan Land Electronic Co. Ltd).

KB/Ru cathode preparation.

KB/Ru composite was synthesized by a reported method (ref. S1). 50 mg of RuCl₃·xH₂O (40 % Ru content) was dissolved in 100 mL of ethylene glycol. 80 mg of KB carbon was added into the solution and was uniformly mixed through an ultrasonic bath. The suspension was refluxed for 3 h at 170 °C. After cooling down, the supernatant was removed and the remnant mixture was centrifuged with deionized water and ethanol several times. The resulting products were dried in a vacuum oven at 80 °C for 12 h. The preparation of KB/Ru-based air electrode is summarized as follow: firstly, KB/Ru (80 wt%), KB (10 wt%) and polyvinylidene fluoride binder (PVDF, 10 wt%) were intimately mixed in an N-methyl-2-pyrrolidone (NMP) solution. After that, the resulting slurry was coated on a carbon paper and the KB/Ru based electrode was dried for 12 h at 100 °C under vacuum to remove residual solvent. The mass loadings of active material in KB/Ru electrodes are ~0.15 mg cm⁻².

KB/Ru flexible cathode preparation.

Firstly, 80 wt % KB/Ru, 10 wt % KB and 10 wt % polyvinylidene fluoride binder (PVDF) were intimately mixed in a N-methyl-2-pyrrolidone (NMP) solution, and the resulting slurry was coated on carbon rope. Finally, the coated electrode was dried for 12 h at 120 °C to remove residual solvent. The mass loadings of active material in flexible KB/Ru electrodes are ~0.15 mg cm⁻².

Li/rGO-Ni flexible cathode preparation.

Firstly, nickel foam strip (~5 cm²) was washed successively with 1 M hydrochloric acid, acetone, and ethanol for 15 minutes and then dried in vacuum drying oven for 12 h. After that, the obtained Ni strip was repeatedly soaked with 5 wt% GO solution for several times and then dried at 80 °C for 12 h to obtain GO modified Ni (GO-Ni) strip. Finally, the dried GO-Ni strip was then immersed into molten Li to produce Li-infused rGO-Ni (Li/rGO-Ni) strip electrode in an Ar-filled glovebox with O₂ and H₂O content below 0.1 ppm. The Li was previously melted in a stainless-steel case on a hot plate at a temperature of 300 °C. After cooled to room temperature, the long strip Li/rGO-Ni was carefully rolled into the fiber-shaped composite electrode.

Precursor solution of gel polymer electrolyte preparation.

4 g Solution A (1 M LiTFSI in TEGDME), 5 g Solution B (1 g PVDF-HFP/4 g NMP) and 3.01 g Solution C (0.01 g HMPP in 3 g TMPET) were well mixed to form the precursor solution.

Detection of the discharge/charge products via XRD and FT-IR technologies.

Firstly, the Li–O₂ battery with KB/Ru electrodes was discharged at a current density of 100 mA g⁻¹ with a fixed capacity of 3000 mAh g⁻¹. After that, the cell was disassembled in a glove box filled with Ar to obtain the discharged electrode. Then, the discharged electrode was further washed with DME for several times and dried under vacuum at room temperature for 5 hours. Next, the discharged electrode was detected by FT-IR and XRD spectra. The KB/Ru catalytic electrodes before discharge and after recharge were detected with the same method.

Coulombic efficiency measurements.

To measure the Li Coulombic efficiency, the obtained Li/rGO-Ni substrate or Cu foil was used as the working electrode and Li metal as the counter electrode with 1.0 M LiTFSI in 1:1 v/v DME and DOL with 2.0 wt% LiNO₃ electrolyte. The cells were first cycled at 0-1 V (*vs* Li⁺/Li) at 0.05 mA for 3 cycles for activation and SEI formation. The following procedures were to deposit the fixed amount of Li (1.0 mAh cm⁻²) at different current densities and stripping Li until the voltage reached up to 1.0 V (*vs* Li⁺/Li) at the same current density.

Characterization instrumentation.

XRD measurements were performed on a Bruker D8 Focus power X-ray diffractometer with Cu K_α radiation. Field emission scanning electron microscopy SEM investigations were conducted using a JSM-6390 microscope from JEOL. Transmission electron microscopy (TEM) experiments were conducted using a JEOL 2011 microscope (Japan) operated at 200 kV. Fourier transform-infrared spectroscopy (FT-IR) tests were performed on a Nicolet 6700 spectrometer. LAND cycler (Wuhan Land Electronic Co. Ltd) was employed for electrochemical tests. EIS experiments and electrodeposition experiments were conducted on an electrochemical workstation (Reference 3000: Gamry). A quadrupole mass spectrometer (NETZSCH QMS 403 C) with leak inlet was connected to a customized Swagelok cell assembly for *in situ* DEMS investigation.



Figure S1 Time-lapse images of Li melt-infusion process into Ni foam (conducted at a heating platform, 300 °C).

As shown in **Figure S1**, the molten Li cannot be loaded on the surface of Ni foam easily due to the poor lithiophilicity. Therefore, only partial surface of Ni foam is covered by molten Li.



Figure S2 Time-lapse images of Li melt-infusion process into GO-Ni composite (conducted at a heating platform, 300 °C).

It can be seen from **Figure S2** that molten Li infuses into GO-Ni matrix in 120 s, which is obviously faster than that in Ni foam (**Figure S3**), suggesting the superior lithiophilicity of GO-Ni film.

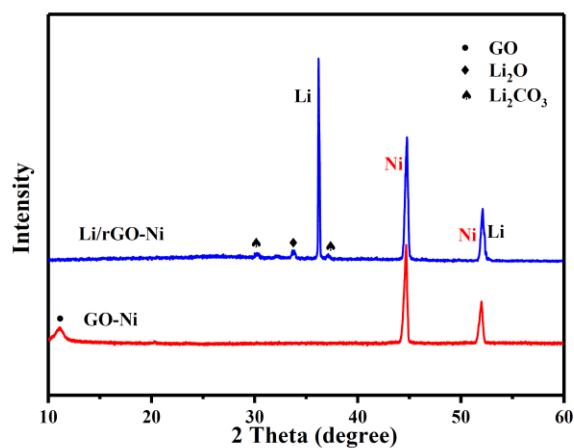


Figure S3 XRD patterns of GO-Ni and Li/rGO-Ni.

As shown in **Figure S3**, compared with the pristine GO-Ni film, there are several additional peaks attributed to metallic Li in the XRD pattern of the Li/rGO-Ni composite, which suggests the successful introduction of Li in the GO-Ni matrix. And the pristine GO-Ni shows a diffraction peak at around 11° , which can be attributed to the (002) plane of GO, indicating the successful introduction of GO into GO-Ni. After thermal infusion process, the typical peak of GO at around 11° has disappeared in the XRD pattern of Li/rGO-Ni.

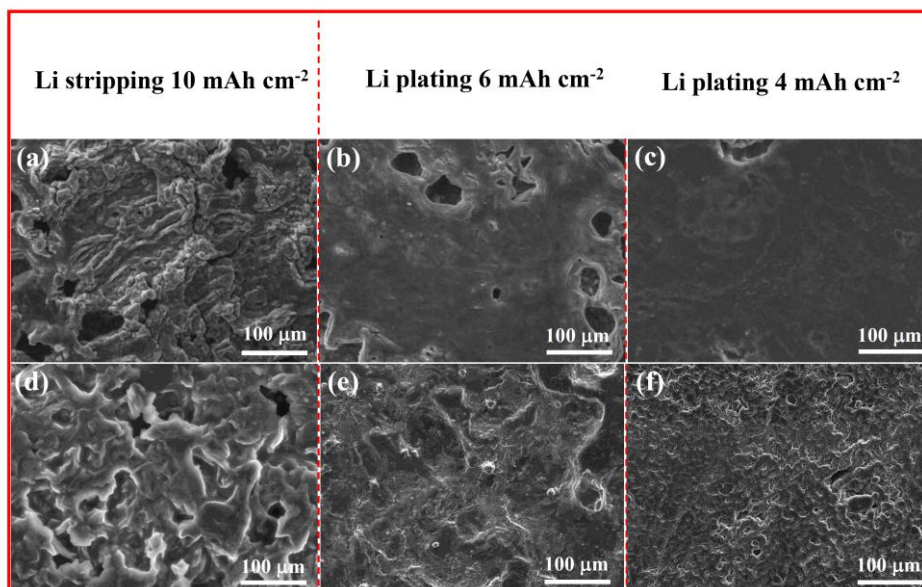


Figure S4 Top SEM images of (a-c) Li/rGO-Ni and (d-f) pure Li electrode at 1 mA cm⁻² after (a, d) stripping away 10 mAh cm⁻², and plating (b, e) 6 mAh cm⁻² and (c, f) 4 mAh cm⁻² Li back, respectively. All the applied current density is 1 mA cm⁻².

As shown in **Figure S4a**, the surface of Li/rGO-Ni becomes rough and the basic framework of GO-Ni also re-emerges with the residual Li particles at the Li stripping capacity of 10 mAh cm⁻². This result indicates that the skeleton of Li/rGO-Ni anode is very stable during the Li stripping process. When 6 mAh cm⁻² Li is deposited back, the voids in this matrix are filled with metallic Li and the surface of Li/rGO-Ni electrode is also uniformly coated with Li (**Figure S4b**), indicating that the rGO-Ni matrix can induce the homogeneous nucleation of metallic Li during the Li plating process. When the additional capacity of 4 mAh cm⁻² Li continues to be plated back, the surface of the ultimate Li/rGO-Ni anode becomes very smooth without any dendritic Li (**Figure S4c**), and is in agreement with the original Li/rGO-Ni electrode (**Figure 1d**). These results demonstrate that the Li-GL/NC-CP anode has the superior reversibility over the Li stripping/plating process. For comparison, the pure Li anode is also tested under the same condition. It can be found from **Figure S4d-f** that the surface of metallic Li electrode becomes very rough and even is covered with several obvious Li dendrites after stripping away and replating back 10 mAh cm⁻² Li, which indicates the inferior cycle stability of Li anode.

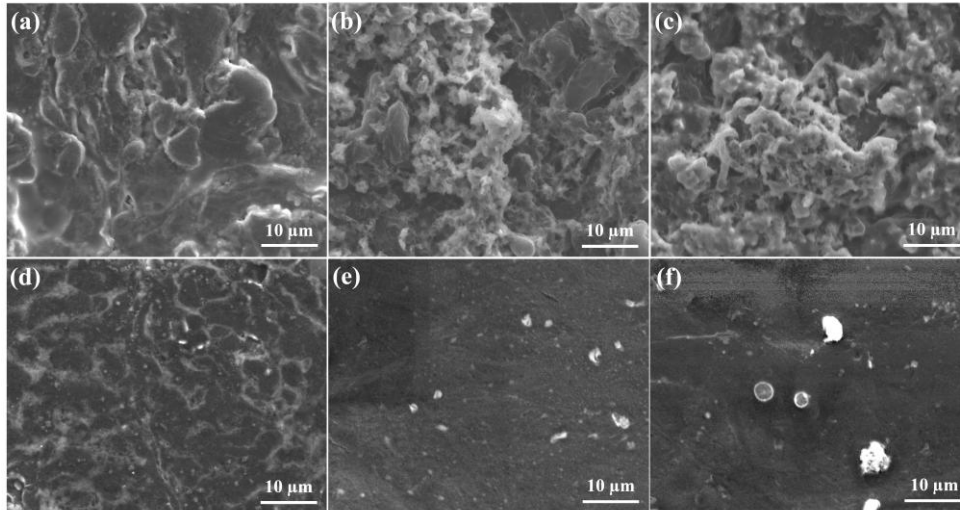


Figure S5 SEM images of (a-c) bare Li and (d-f) Li/rGO-Ni anodes at a fixed capacity of 1 mAh cm⁻² after 20 Li stripping/plating cycles under different current densities: (a, d) 1 mA cm⁻² of (b, e) 3 mA cm⁻² (c, f) 5 mA cm⁻².

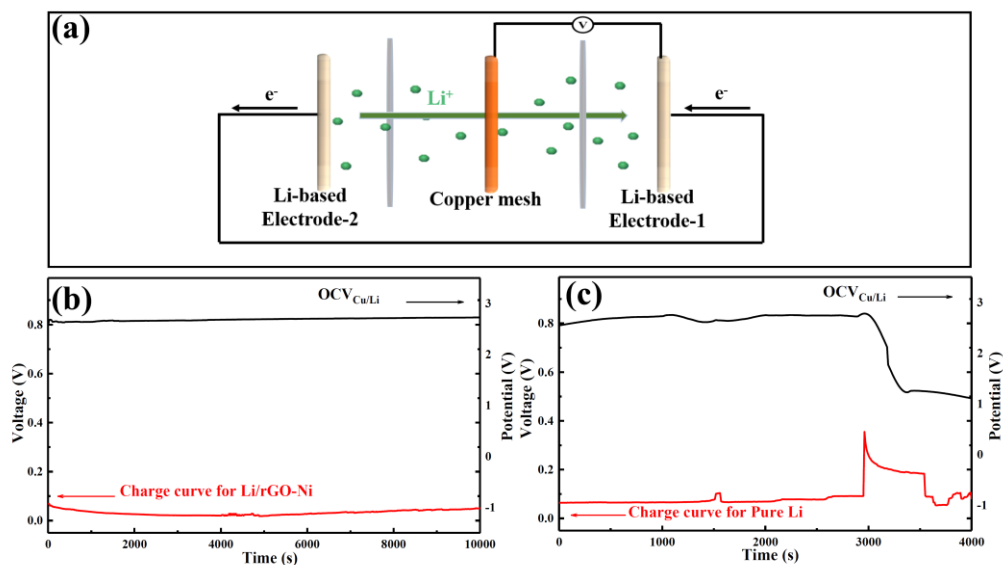


Figure S6 (a) The schematic diagrams and the corresponding safety tests of Li/rGO-Ni and pure Li electrodes. Safety tests of (b) Li/rGO-Ni and (c) pure Li anodes.

In this test, Li/rGO-Ni (Li)|Cu wire|Li/rGO-Ni (Li) symmetrical cell was assembled. These symmetric cells are continuously charged at 5 mA cm^{-2} and the open circuit voltage (OCV) of Cu wire|Li/rGO-Ni (Li) is also recorded at the same time. As shown in **Figure. S6b**, the charge profile of Li/rGO-Ni based cell is very flat and the OCV of Li/rGO-Ni|Cu can also stably maintain $\sim 2.75 \text{ V}$ over 10000 s, while Li/rGO-Ni based battery exhibits the fluctuating curve and the OCV of Li|Cu rapidly declines at 3000 s (**Figure. S6c**). Sudden drop in voltage is due to the growth of Li dendrites piercing the membrane, resulting in short circuit of Li|Cu wire half-cell.

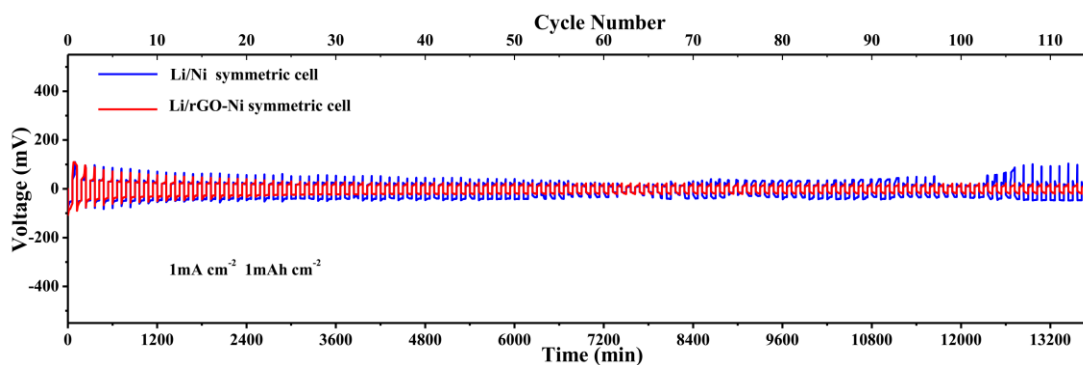


Figure S7 Cycle performance of Li/Ni and Li/rGO-Ni electrodes in symmetrical cells under the limited stripping/plating capacity of 1 mAh cm^{-2} at 1 mA cm^{-2} .

As shown in **Figure S7**, the Li stripping/plating platforms of Li/rGO-Ni electrode are still almost constant with voltage polarization around $\sim 40 \text{ mV}$ over 110 cycles, while the voltage profiles of Li/Ni electrode have the irregular and dramatic oscillation after only 60 cycles. Moreover, the overpotentials of Li/Ni electrode are always higher than these of the Li/rGO-Ni electrode during 110 cycles.

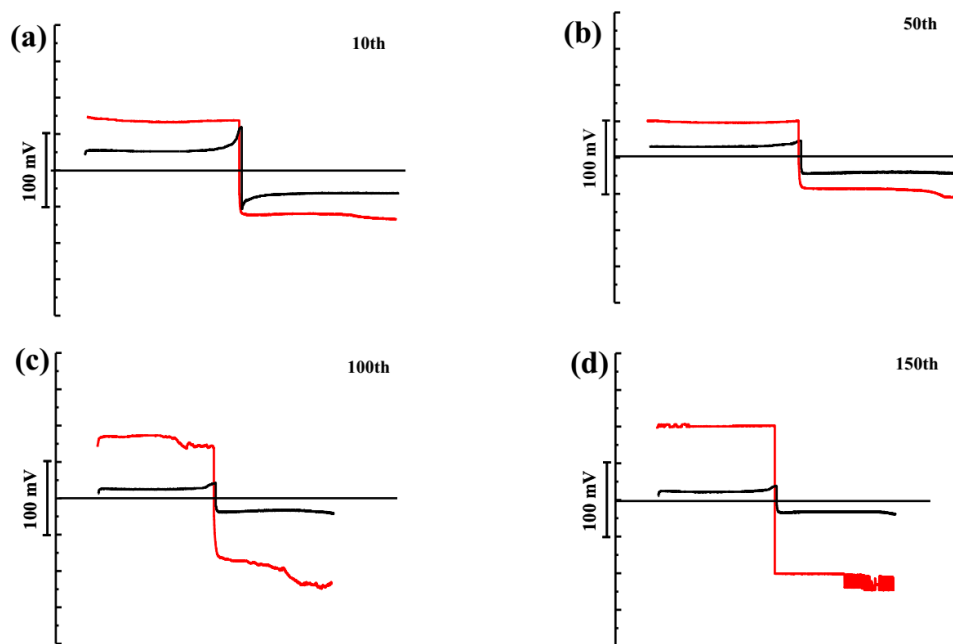


Figure S8 Comparisons of voltage profiles of Li/rGO-Ni and bare Li electrodes in symmetrical cells under a current density of 1 mA cm^{-2} for 1 mAh cm^{-2} at the (a) 10th, (b) 50th, (c) 100th and (d) 150th cycle, respectively.

As shown in **Figure S8**, the symmetrical cell with Li/rGO-Ni exhibits stable voltage profiles with the average overpotential of $\sim 40 \text{ mV}$. However, the bare Li shows fluctuant voltage profile with large overpotential of almost 200 mV after 150 cycles.

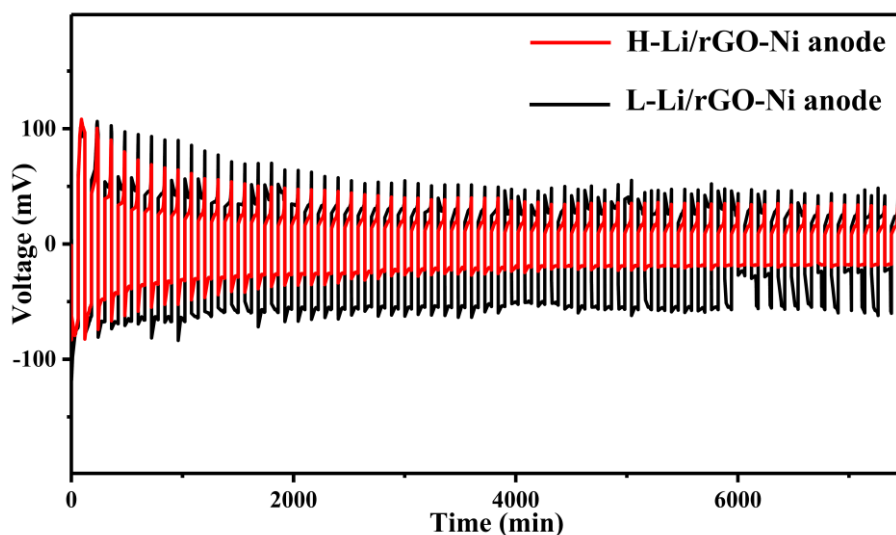


Figure S9 Cycle stability of H-Li/rGO-Ni and L-Li/rGO-Ni anodes in symmetrical cells at the current density of 1 mA cm^{-2} with the limited stripping/plating capacity of 1.0 mAh cm^{-2}

As shown in **Figure S9**, both Li/rGO-Ni (Fig. 3a) and H-Li/rGO-Ni composite electrode almost exhibits the constant discharge/charge curves with very low voltage hysteresis ($\sim 40 \text{ mV}$) over 60 cycles at the current density of 1 mA cm^{-2} . Although the performance of H-Li/rGO-Ni anode is similar to Li/rGO-Ni anode, more Li amount undoubtedly increases the weight and cost. On the contrast, L-Li/rGO-Ni anode exhibits poor cycling stability and even shows the obvious voltage fluctuation after 50 cycles. These results indicate that the Li amount in Li/rGO-Ni anode is optimized.

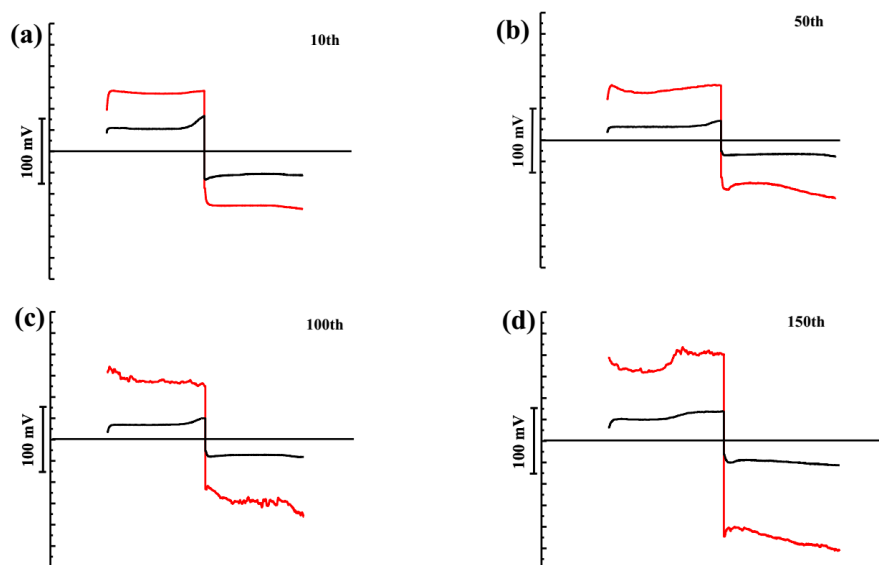


Figure S10 Comparisons of voltage profiles of Li/rGO-Ni and bare Li electrodes in symmetrical cells under a current density of 3 mA cm^{-2} for 1 mAh cm^{-2} at the (a) 10th, (b) 50th, (c) 100th and (d) 150th cycle, respectively.

As shown in **Figure S10**, the symmetrical cell with Li/rGO-Ni exhibits stable voltage profiles with the average overpotential of $\sim 95 \text{ mV}$. However, the bare Li shows fluctuant voltage profile with large overpotential of almost 360 mV after 100 cycles.

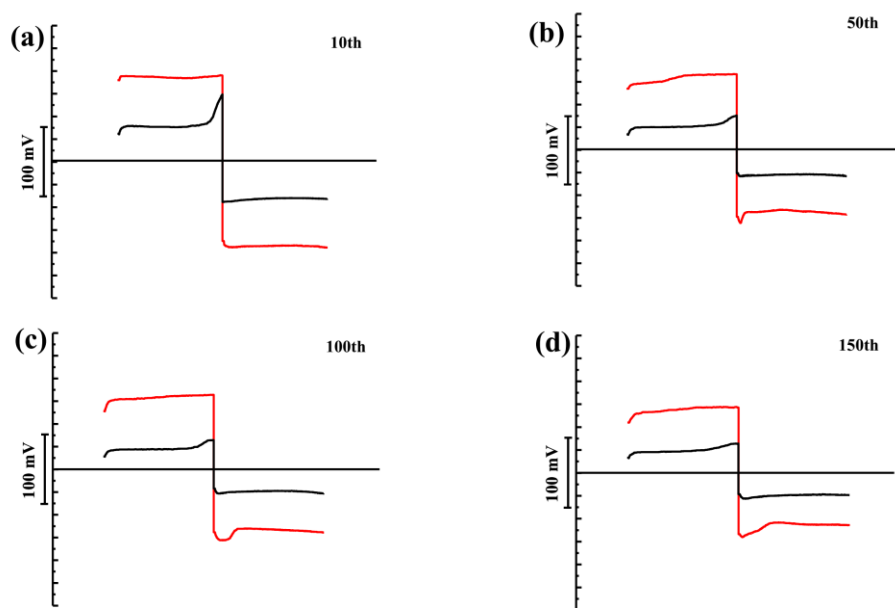


Figure S11 Comparisons of voltage profiles of Li/rGO-Ni and bare Li electrodes in symmetrical cells under a current density of 5 mA cm^{-2} for 1 mAh cm^{-2} at the (a) 10th, (b) 50th, (c) 100th and (d) 150th cycle, respectively.

As shown in **Figure S11**, the symmetrical cell with Li/rGO-Ni exhibits stable voltage profiles with the average overpotential of $\sim 120 \text{ mV}$. However, the bare Li shows fluctuant voltage profile with large overpotential of almost 300 mV after 150 cycles.

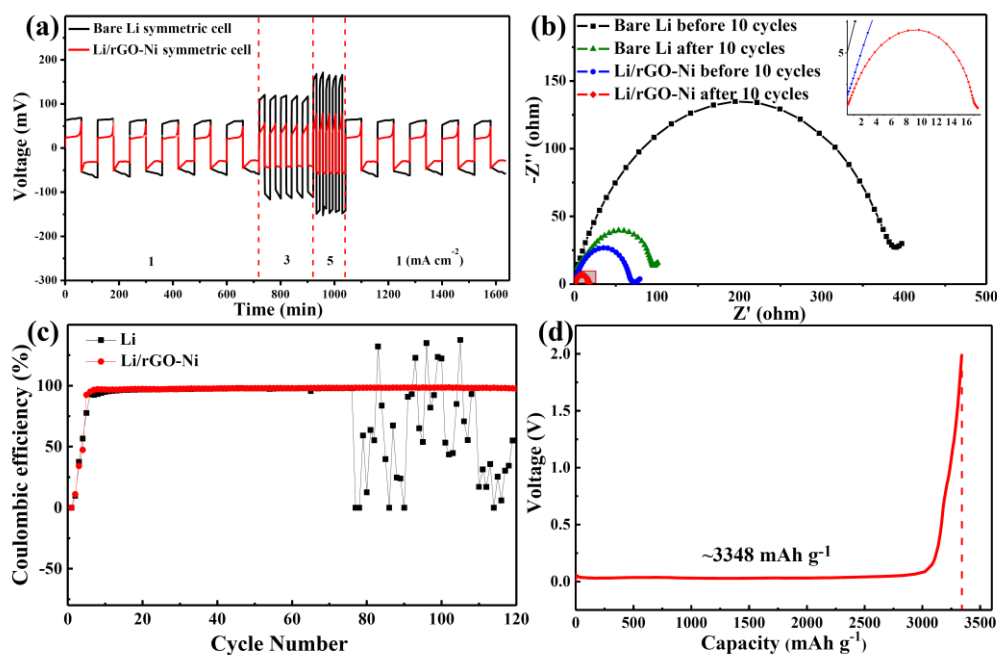


Figure S12 (a) Rate performance for the Li/rGO-Ni and bare Li anodes in symmetrical batteries; (b) Nyquist plots of the symmetrical cells with Li/rGO-Ni and bare Li anodes and nyquist plots of the symmetrical cells with Li/rGO-Ni and bare Li anodes after 10 cycles; (c) Comparison of Coulombic efficiencies of Li/rGO-Ni and Li electrodes at 1 mA cm^{-2} with a lithiation capacity of 1 mAh cm^{-2} ; (d) The voltage profile of the Li/rGO-Ni anode at a current density of 0.5 mA cm^{-2} over the Li stripping process.

As shown in **Figure S12d**, the interfacial resistance of Li/rGO-Ni anode after 10 cycles also shows a decrease compared with the pristine Li/rGO-Ni anode. The drop in interfacial resistance of Li/rGO-Ni anode may be attributed to the unimpeded charge transfer process from its increased specific surface area (ref. S2, ref. S4). The decomposition of the native passivation layers on the surface of Li/rGO-Ni anode, redistribution of metallic Li in the whole skeleton of rGO-Ni and so on during cycles may increase the surface area (ref. S3 and S12). In addition, the superior interface stability of Li/rGO-Ni ensure that its interfacial resistances are always smaller than pure Li over cycles. Moreover, many recently reported high-performance Li-based anodes also show the similar decrease trend over cycles (ref. S3 and S13).

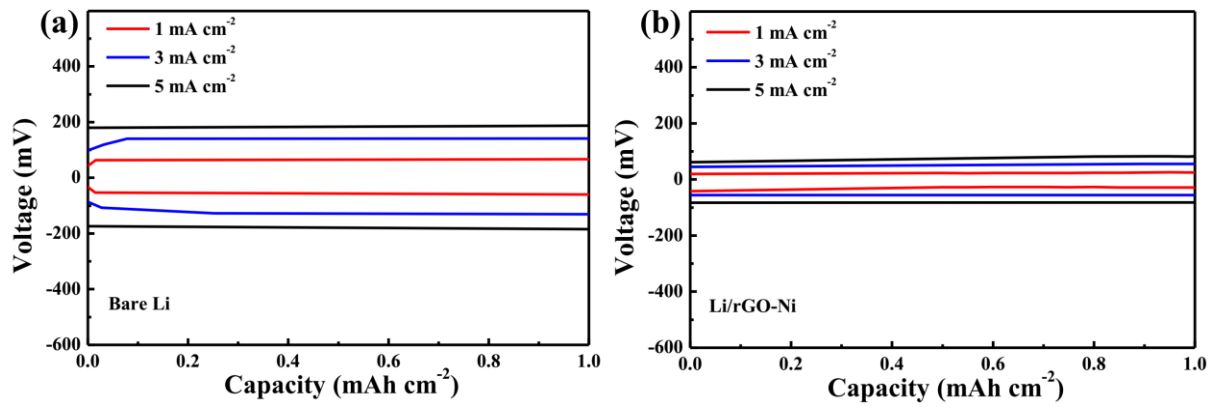


Figure S13 Voltage profiles of (a) bare Li and (b) Li/rGO-Ni based symmetric cells at various current density from 1 to 5 mA cm⁻².

As shown in **Figure S13**, the overpotentials of Li/rGO-Ni in symmetric cells at the current densities of 1.0, 3.0 and 5.0 mA cm⁻² are within 60, 110 and 170 mV, respectively, which are smaller than Li anode under all these current densities.

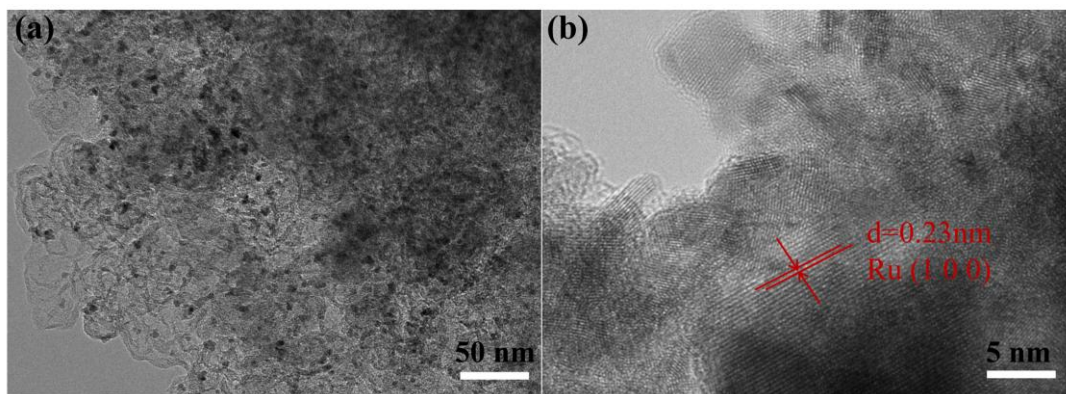


Figure S14 (a) TEM image and (b) HR-TEM image of the KB/Ru.

As shown in **Figure S14**, there are large amounts of Ru particles distributed on the surface of KB carbon. Clear lattice stripes of 0.23 nm corresponding to the facet of (100) Ru can be seen in the HR-TEM image.

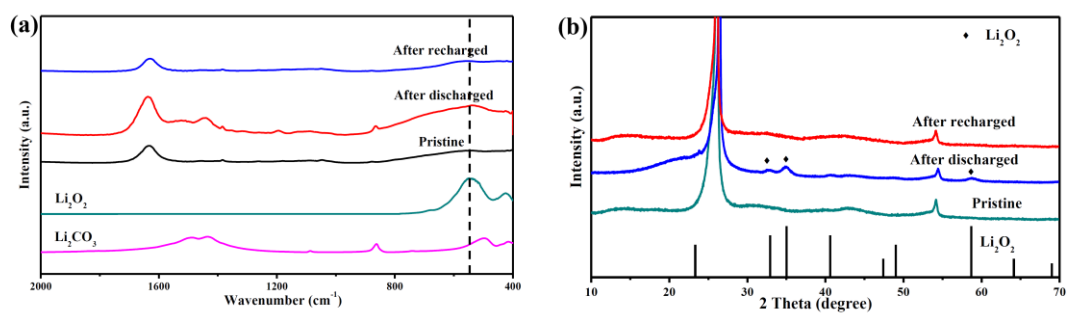


Figure S15 (a) FT-IR of the KB/Ru cathodes at different stages. (b) XRD patterns of the KB/Ru cathodes at different stages.

As shown in **Figure S15**, Li₂O₂ is the main product at the end of discharge and then have been disappeared over the charge process.

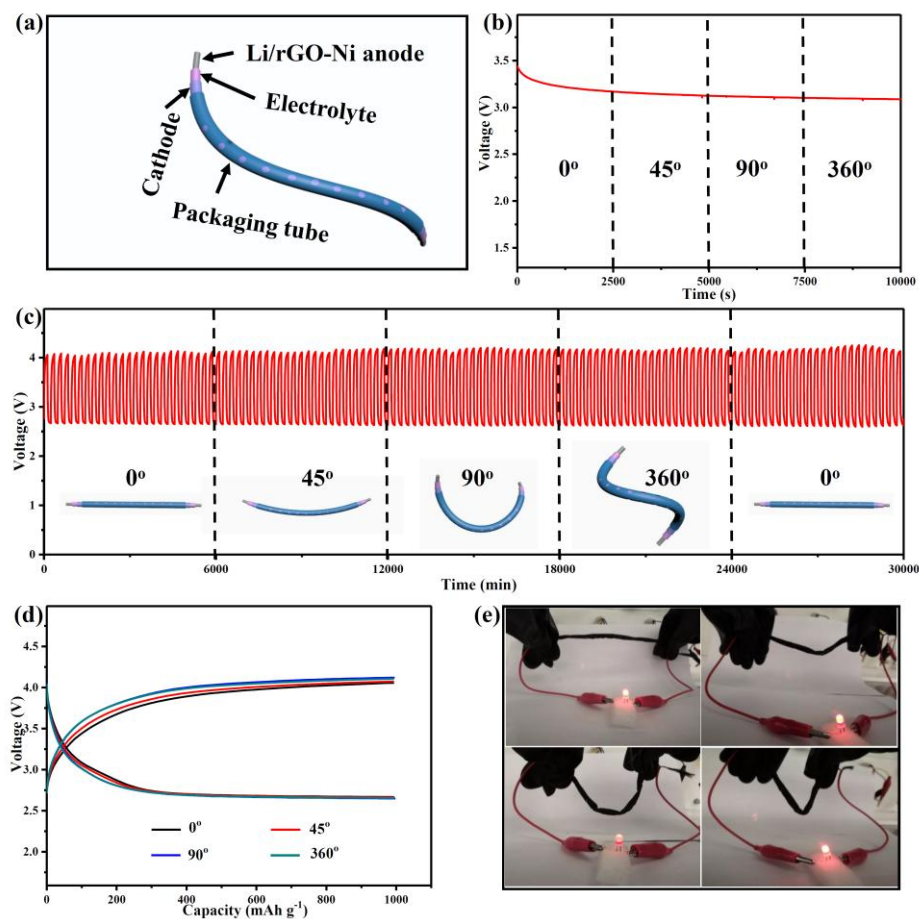


Figure S16 (a) The schematic diagram of flexible Li–O₂ battery using Li/rGO-Ni anode; (b) Open-circuit voltage curve of flexible Li/rGO-Ni based Li–O₂ battery; (c) Cycle performance at a current density of 200 mA g⁻¹ under different bending conditions: 0°, 45°, 90°, 360° and re-bending to 0° and (d) the corresponding detailed charge/discharge curves of the flexible Li/rGO-Ni-based Li–O₂ battery under different bending conditions: 0°, 45°, 90°, 360°; (e) Photograph of LED driven by the flexible Li/rGO-Ni-based Li–O₂ battery under different bending conditions.

Table S1 Comparison of electrochemical performances for Li-based anodes

Materials	Electrolyte	Current density	Overpotential(mV)	Cycle time(h)	References
TiC/C/Li	1M LiTFSI in 1:1 v/v DME and DOL with 1 wt% LiNO ₃	1mA 1mAh cm ⁻²	100	400	Ref. S4
CNF-Sn-5%@Li	1 M LiTFSI in DOL/DME in a volume ratio of 1:1 with 0.2 M LiNO ₃	1mA 1mAh cm ⁻²	75	650	Ref. S5
Li@CDG-sponge	1M LiTFSI in 1:1 v/v DME and DOL with 1 wt% LiNO ₃	1mA 1mAh cm ⁻²	85	780	Ref. S6
CONF-Li	1 M LiTFSI in DOL/DME in a volume ratio of 1:1 with 0.1 M LiNO ₃	1mA 1mAh cm ⁻²	100	260	Ref. S7
Li/C-wood	1.0 M LiPF ₆ in EC/DEC (volume ratio 1:1)	1mA 1mAh cm ⁻²	200	300	Ref. S8
Li-Mn/G foam	1M LiTFSI in 1:1 v/v DME and DOL with 1 wt% LiNO ₃	1mA 1mAh cm ⁻²	100	1600	Ref. S9
3D Li@CuLi	1 M LiPF ₆ in DMC of 1: 1: 1 volume ratio + 10% FEC	3mA 1mAh cm ⁻²	100	133	Ref. S10
Li/C anode	1.0 M LiPF ₆ in EC/DEC (volume ratio 1:1)	3mA 1mAh cm ⁻²	190	54	Ref. S11
Li-rGO anode	1 M LiPF ₆ in EC/DMC of 1: 1 volume ratio + 2% VC	3mA 1mAh cm ⁻²	80	69	Ref. S12
Li-Ni anode	1.0 M LiPF ₆ in EC/DMC/EMC (volume ratio 1:1:1)	1mA 1mAh cm ⁻²	100	200	Ref. S13
CFC/Li electrode	1.0 M LiPF ₆ in EC/DEC (volume ratio 1:1)	1mA 1mAh cm ⁻²	96	400	Ref. S14
CF/Ag-Li	1.0 M LiPF ₆ in EC/DEC (volume ratio 1:1)	1mA 1mAh cm ⁻²	100	400	Ref. S15
Li/rGO-Li	1M LiTFSI in 1:1 v/v DME and DOL with 1 wt% LiNO ₃	1mA 1mAh cm ⁻²	40	230	This work

As listed in **Table S1**, Li/rGO-Ni anode shows small overpotential and long cycling life, which is better than most of the recently reported pre-stored Li metal anodes.

Reference

- ref. S1:** S. X. Yang, Y. Qiao, P. He, Y. J. Liu, Z. Cheng, J. J. Zhu, H. S. Zhou, *Energy Environ. Sci.*, 2017, 10, 972–978.
- ref. S2:** R. Zhang, X. Shen, X.-B. Cheng, Q. Zhang. *Energy Storage Mater.*, 2019, 23, 556–565.
- ref. S3:** Z. Zhang, J. L. Wang, X. F. Yan, S. L. Zhang, W. T. Yang, Z. H. Zhuang, W.-Q. Han, *Energy Storage Mater.*, 2020, 29, 332–340.
- ref. S4:** S. F. Liu, X. H. Xia, Y. Zhong, S. J. Deng, Z. J. Yao, L. Y. Zhang, X. B. Cheng, X. L. Wang, Q. Zhang, J. P. Tu, *Adv. Energy Mater.*, 2018, 8, 1702322.
- ref. S5:** T. C. Liu, J. L. Hu, C. L. Li, Y. Wang, *ACS Appl. Energy Mater.*, 2019, 2, 4379-4388.
- ref. S6:** J. Li, P. C. Zou, S. W. Chiang, W. T. Yao, Y. Wang, P. Liu, C. W. Liang, F. Y. Kang, C. Yang, *Energy Storage Mater.*, 2020, 24, 700-706.
- ref. S7:** X. Y. Yue, W. W. Wang, Q. C. Wang, J. K. Meng, Z. Q. Zhang, X. J. Wu, X. Q. Yang, Y. N. Zhou, *Energy Storage Mater.*, 2018, 14, 335-344.
- ref. S8:** Y. Zhang, W. Luo, C. W. Wang, Y. J. Li, C. J. Chen, J. W. Song, J. Q. Dai, E. M. Hitz, S. M. Xu, C. P. Yang, Y. B. Wang, L. B. Hu, *P. Natl. Acad. Sci. USA*, 2017, 114, 3584-3589.
- ref. S9:** B. Z. Yu, T. Tao, S. Mateti, S. G. Lu, Y. Chen, *Adv. Funct. Mater.*, 2018, 28, 1803023.
- ref. S10:** K. R. Adair, M. Iqbal, C. H. Wang, Y. Zhao, M. N. Banis, R. Y. Li, L. Zhang, R. Yang, S. G. Lu, X. L. Sun, *Nano Energy*, 2018, 54, 375-382.
- ref. S11:** Z. Liang, D. C. Lin, J. Zhao, Z. D. Lu, Y. Y. Liu, C. Liu, Y. Y. Lu, H. T. Wang, K. Yan, X. Y. Tao, Y. Cui, *P. Natl. Acad. Sci. USA*, 2016, 113, 2862-2867.
- ref. S12:** D. C. Lin, Y. Y. Liu, Z. Liang, H. W. Lee, J. Sun, H. T. Wang, K. Yan, J. Xie, Y. Cui, *Nat. Nanotechnol.*, 2016, 11, 626-632.
- ref. S13:** S. S. Chi, Y. C. Liu, W. L. Song, L. Z. Fan, Q. Zhang, *Adv. Funct. Mater.*, 2017, 27, 1700348.

ref. S14: S. F. Liu, X. H. Xia, Z. J. Yao, J. B. Wu, L. Y. Zhang, S. J. Deng, C. G. Zhou, S. H. Shen, X. L. Wang, J. P. Tu, *Small Methods*, 2018, 2, 1800035.

ref. S15: R. Zhang, X. Chen, X. Shen, X.-Q. Zhang, X.-R. Chen, X.-B. Cheng, C. Yan, C.-Z. Zhao, Q. Zhang, *Joule*, 2018, 2, 764-777.